A 3-D Numerical Study of Pinhole Diffraction to Predict the Accuracy of EUV Point Diffraction Interferometry

K. A. Goldberg[a,b], E. Tejnil[c], J. Bokor[a,c]

[a]*Center for X-ray Optics, Lawrence Berkeley National Laboratory, Berkeley, CA 94720*
[b]*Physics Department, University of California, Berkeley, CA 94720*
[c]*EECS Department, University of California, Berkeley, CA 94720*

Abstract

A three-dimensional (3-D) electromagnetic field simulation is used to model the propagation of extreme ultraviolet (EUV), 13 nm wavelength, light through sub-1500 Å diameter pinholes in a highly absorptive medium. Deviations of the diffracted wavefront phase from an ideal sphere are studied within 0.1 numerical aperture, to predict the accuracy of EUV point diffraction interferometers used in at-wavelength testing of nearly diffraction-limited EUV optical systems. Aberration magnitudes are studied for various 3-D pinhole models, including cylindrical and conical pinhole bores.

Key Words

Interferometry, Optical Testing, Diffraction Theory, Pinhole Diffraction

Introduction

Point diffraction interferometers [1, 2, 3, 4] are a class of common-path interferometers that generate a spherical reference wavefront by diffraction. They are presently used to perform at-wavelength optical wavefront measurements of nearly diffraction-limited extreme ultraviolet (EUV) optical systems where sub-nanometer wavefront aberration tolerances are required [5, 6]. The reference wavefront is created by diffraction from a tiny pinhole placed near the focus of a coherently illuminated optical system under test. This diffracted wavefront interferes with the wavefront transmitted by the test optic, and the measured interference fringe pattern, recorded far from the focus, can be analyzed to reveal aberrations in the test optic. The fringe pattern reveals the optical path difference between the test and reference wavefronts. Therefore, the accuracy of the measurement relies on the quality of the diffracted spherical reference wavefront over the numerical aperture (NA) of interest.

A detailed simulation of pinhole diffraction enables the prediction of non-spherical components in the diffracted wavefront phase, and allows estimation of the measurement accuracy limits. Several methods have been developed to study diffraction from a variety of aperture shapes with various boundary conditions [7, 8], yet no general analytical treatment addresses diffraction through pinholes in a highly absorptive medium, with the range of non-ideal shapes that serve as reasonable physical models for the experimental pinholes used in EUV point diffraction interferometry near 13 nm wavelength [5]. The introduction of the three-dimensional pinhole structure and the inclusion of the polarization of the incident light motivate the use of numerical solutions based on detailed simulations of the vector electromagnetic field in the vicinity of the pinhole.

Modeling the electromagnetic field

Pinholes with diameters ranging from 500 – 2000 Å (~3 –15 λ), fabricated by electron beam lithography in a highly absorptive cobalt membrane approximately 900 Å (~7 λ) thick [9], are considered in this study because they are suitable for testing optical systems with NA around 0.1 at 13 nm wavelength. The three-

Table 1. Parameters of the pinhole simulations.

Wavelength	λ = 13.55 nm (91.5 eV)
Illumination	Uniform plane wave, normal incidence, plane polarized.
Simulation Domain size	2306 Å x 2306 Å x 1152 Å = 17 λ x 17 λ x 8.5 λ
Simulation nodes	λ/15 spacing, 2×10^6 total nodes
Pinhole Diameters	500 Å - 1500 Å
Cobalt membrane	thickness, 900 Å = 6.64 λ density, 8.9 g/cm^3
Index of refraction	$n = 1 - \delta + i\beta$ $= 1 - 0.06589 + 0.06574i$

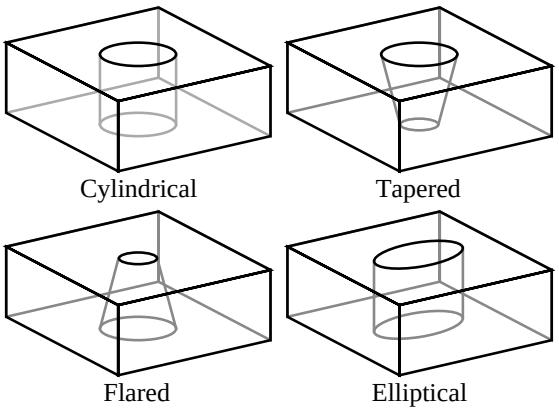

Figure 1. Geometry of the pinhole simulation domains, showing the orientation of a pinhole in the cobalt membrane. In the simulations, linearly polarized monochromatic light, of 13.55 nm wavelength is normally incident from above.

dimensional electromagnetic field in the vicinity of the pinhole was calculated using TEMPEST 3D [10], a time-domain, vector electromagnetic field simulation computer program. Calculations were performed on a range of pinhole geometry models including, cylindrical and conical pinholes, and elliptical pinholes of uniform cross-section. Variations of the field incident on the pinhole were neglected: across the small simulation domain, uniform, normally incident, plane-wave illumination, with linear polarization along the *x*-axis was assumed.

Parameters of the simulation are listed in Table 1. The simulation domain, which exploits the two-fold symmetry of the pinhole models, contains a cobalt membrane in vacuum with a thin layer of free space above and below. TEMPEST 3D uses periodic boundary conditions in the *x* and *y* directions, thereby forming a square array of virtual pinholes with center-to-center spacing of 2306 Å for the parameters of interest. This separation distance is great enough to reduce overlapping fields from neighboring pinholes in the periodic domain, and thus allow treatment as if from an isolated pinhole.

The propagation of EUV light in cobalt is characterized by rapid extinction: the 1/*e* intensity transmission depth is 164 Å (1.2 λ), and the relative transmission through 900 Å is 4×10^{-3}. This attenuation further reduces the effects of overlapping fields from neighboring domains. The diffraction pattern of standing waves formed within the open pinholes is shown in Fig. 2.

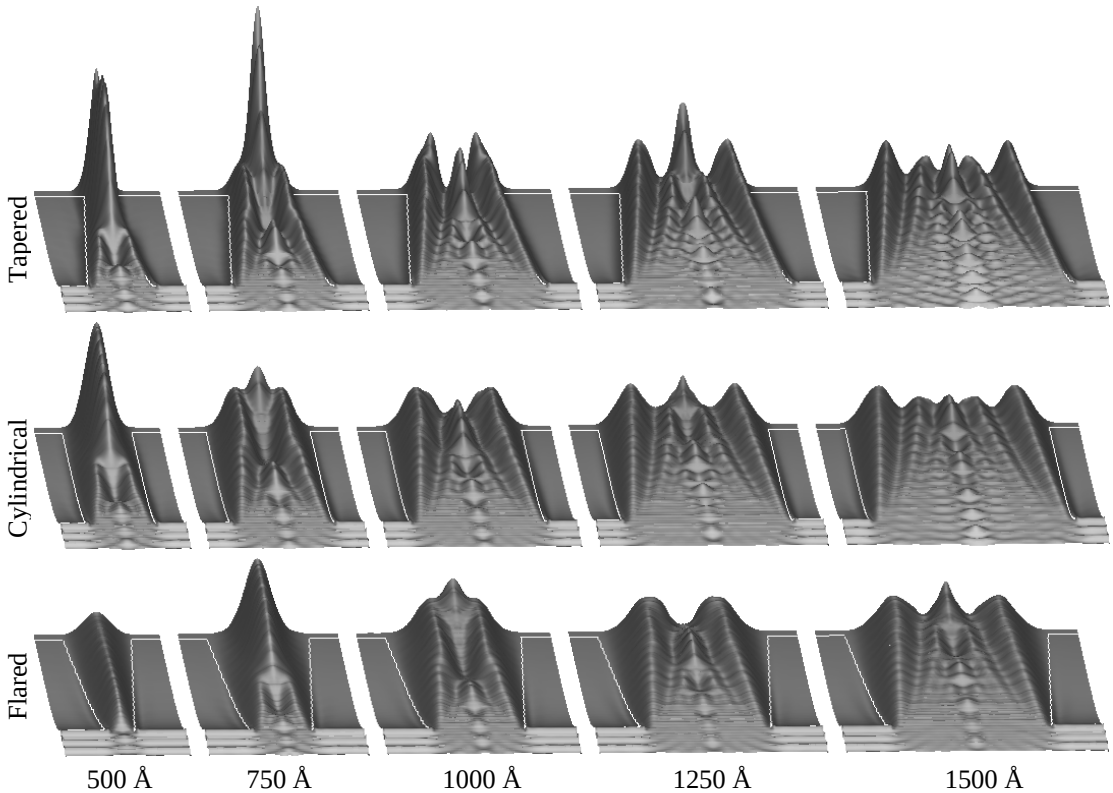

Figure 2. Calculated electric field intensity patterns showing diffraction within the pinhole, and attenuation in the cobalt membrane. Surface heights represent the electric field intensity in a plane containing the axis of the pinhole and the direction of the electric field polarization. The light propagates from the bottom of each image to the top. White lines on the surfaces represent the boundaries of the cobalt.

Table 2. Far-field diffraction of a spherical wavefront from a circular aperture, in the Kirchoff scalar diffraction approximation.

d (Å)	500	750	1000	1250	1500	1750
NA	0.33	0.22	0.17	0.13	0.11	0.094

Propagation to far-field

The diffracted wavefront was calculated within 0.1 NA by numerical propagation of the calculated electric field to a spherical surface 10 cm away. This distance represents the far-field experimentally, and corresponds to the position of the detector in the EUV point diffraction interferometer [5]. The *x*-polarized component of the electric field calculated 27 Å (λ/5) below the cobalt membrane was used as the initial field for the numerical propagation. In the absence of a *y*-polarized component, the *x*-polarized component of the electric field, across the initial *x*-*y* plane is sufficient to completely and uniquely describe the propagated field [11]. The propagation was performed with a two-dimensional Fourier transform that approximates the Fresnel-Kirchoff diffraction formula for far-field diffraction [8].

The propagated field may be described as the superposition of the *diffracted* field and the incident *uniform* field which is transmitted through the cobalt membrane. To isolate the diffracted field, a uniform component of the field, representing only the attenuated transmitted field, was subtracted before the propagation was performed. Isolation of the diffracted field enables the imposition of the boundary condition that the diffracted field becomes arbitrarily small away from the pinhole.

Rapid extinction in the cobalt membrane of all light not transmitted through the open pinhole allows the use of a relatively small domain size in these calculations. An estimate of the total power *outside* of the simulation domain determines the uncertainty in the calculation of the diffracted field. Based on the field magnitude at the edge of the domain and the rate of field attenuation away from the pinhole, the uncertainty in the diffracted field is estimated to be 10^{-4}, relative to a unit intensity incident field. Further study is required to fully characterize the uncertainty introduced by the small domain size.

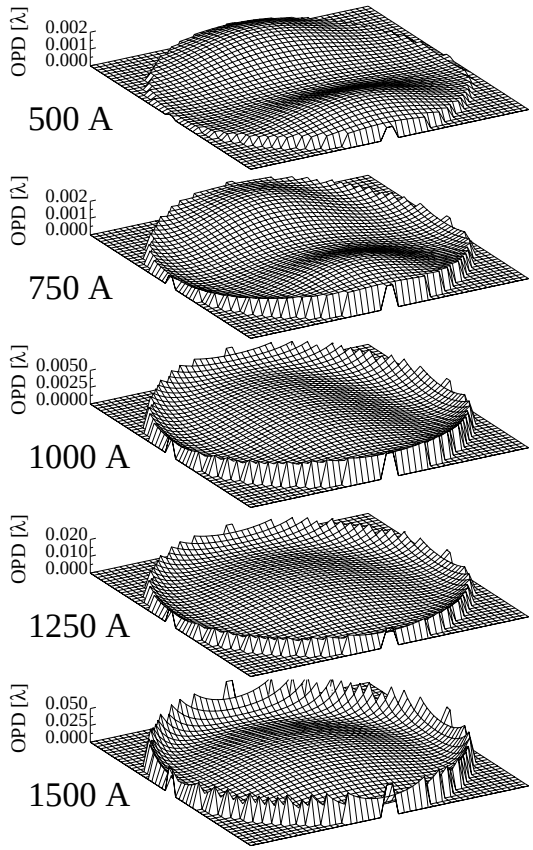

Figure 3. Calculated wavefronts diffracted by cylindrical pinholes. The optical path difference (OPD) between the diffracted wavefront and a perfect, spherical wavefront is shown.

The diffracted wavefront

We characterize the reference wavefront aberrations relative to an ideal spherical wavefront, within 0.1 NA. A first approximation to the far-field wavefront diffracted from the experimental pinhole is the diffraction of a coherent beam from a simple circular aperture in a planar screen, based on the Kirchoff model of scalar diffraction theory [8]. It predicts a spherical reference wavefront covering the central portion of a diffracted Airy pattern, bounded by the first diffraction minimum. Based on this result, a pinhole of diameter, *d*, diffracts a spherical wavefront that fills NA = sinθ = 1.22 λ/*d*, as shown in Table 2.

In each simulation case, the phase of the diffracted wavefront was fit to a series of Zernike polynomials [12, 13] over 0.1 NA. The four lowest-order polynomials that describe the displacement of the coordinate system from the wavefront center of curvature, were removed from this analysis. Pinholes from which the remaining peak-to-valley (P-V) wavefront aberration was larger than 0.15 λ were rejected from consideration in this study. This included all pinholes larger than 1500 Å diameter.

Uniform and conical bore

In addition to a simple cylindrical bore, two conical bore models, tapered (narrower at the exit) and flared (wider at the exit), are studied in this article. For both of the conical models, the cone half-angle is 10°. The five pinhole diameters studied here are 500, 750, 1000,

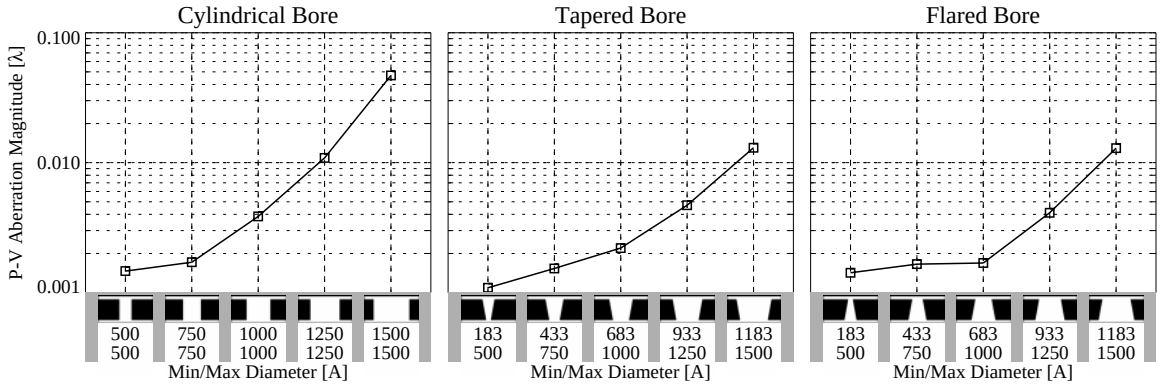

Figure 4. Calculated P-V wavefront aberrations within 0.1 NA for three pinhole bore shape models, and five different diameters. Pinhole cross-sections, parallel to the polarization vector, are shown above the *x*-axis labels: black represents the cobalt membrane, white is empty space.

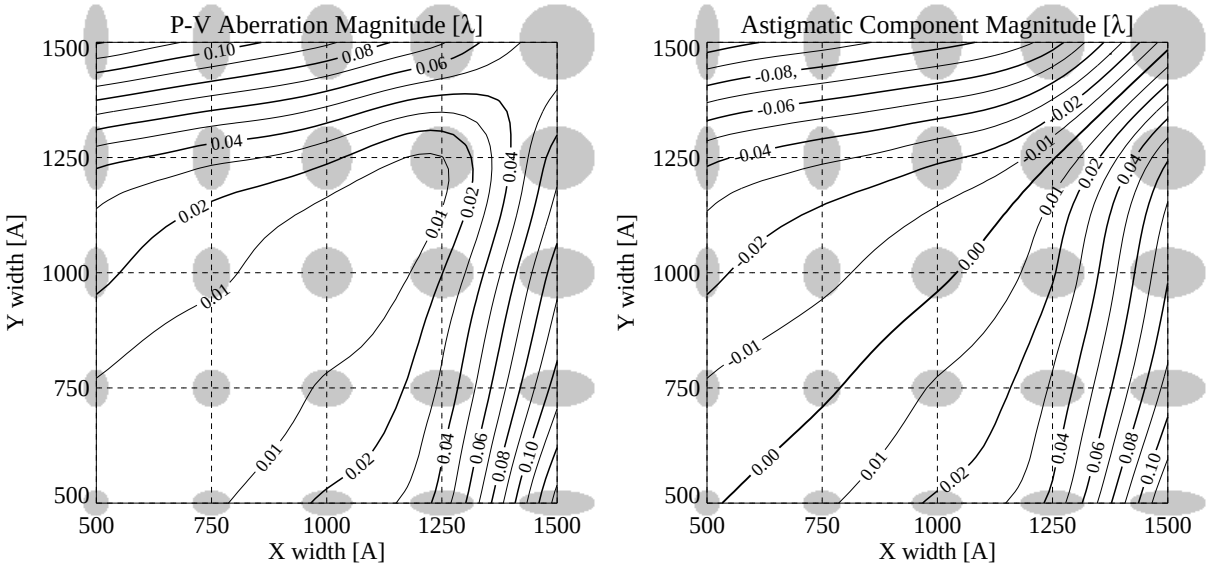

Figure 5. Calculated P-V aberrations (left) of diffracted wavefronts, within 0.1 NA, for elliptical pinhole bores. The pinhole shapes are shown in gray behind their appropriate locations on the plot. Pinhole ellipticity introduces a small amount of astigmatism (right) into the diffracted wavefront.

1250, and 1500 Å. Conical pinholes are labeled by their *maximum* diameters.

Calculated wavefronts diffracted by the cylindrical pinholes are plotted in Fig 3. Wavefronts diffracted by the two smallest pinholes reveal a small astigmatic component, while the largest pinholes diffract wavefronts dominated by rotationally symmetric aberrations.

The calculated P-V wavefront aberration magnitudes are plotted in Fig. 4 for each of the pinhole bore shapes and diameters studied. Within this range, the P-V aberration magnitude is an increasing function of the pinhole size. The dominant wavefront aberration components for the larger pinholes are rotationally symmetric. However, a small astigmatic (cos 2θ) component, less than 0.02 λ P-V, is present in each diffracted wavefront.

The asymmetric wavefront components in diffraction from circular pinholes come from the polarization of the incident field. Electric field components parallel and perpendicular to the walls of the pinhole satisfy different boundary conditions: parallel fields are continuous across the boundary, perpendicular fields are discontinuous. The field emerging from the pinhole is not rotationally symmetric, but owing to reflection symmetry across the *x*- and *y*-axes, it contains *astigmatic* components.

Elliptical bore

A series of simulations was conducted to investigate the effect of elliptical pinhole cross-sections on the

diffracted wavefront. P-V aberration magnitudes are shown in Fig. 5, for 25 width and ellipticity combinations. The aberration magnitudes increase with pinhole size, as expected. Elliptical pinhole wavefronts show greater aberration magnitudes in the direction of the pinholes' major axis, giving rise to non-rotationally symmetric aberrations separate from the field polarization effects described above. In this case, polarization effects also contribute an astigmatic component to the diffracted wavefront. Figure 5 also shows the overall magnitude of these astigmatic components. Since this term depends on $\cos 2\theta$, a negative sign of the coefficient indicates rotation by 90°.

Conclusion

Calculated EUV wavefronts diffracted into 0.1 NA by 500–1500 Å pinholes in a cobalt membrane show aberrations that increase as a function of pinhole size. Even in the presence of a slightly conical bore, or an elliptical cross-section, the diffracted wavefronts are spherical to within 0.01 waves from 1250 Å pinholes, and within 0.002 waves from sub-750 Å circular pinholes. Polarization and pinhole ellipticity both introduce astigmatic components into the diffracted wavefront.

To the extent that these pinhole models correctly represent experimental conditions, measurements of aberrated spherical wavefronts using EUV point diffraction interferometry may be limited to an accuracy of a few thousandths of a wavelength when pinholes as small as 500 Å are used — substantially smaller than the diffraction-limited resolution of the test optics.

Acknowledgments

This work was partially supported by the National Center for Supercomputing Applications, and utilized the Connection Machine Model-5 (CM-5) at the NCSA. Additional support was provided by ARPA Advanced Lithography Project, the DoE office of Basic Energy Sciences, SRC, and an Intel Foundation Graduate Fellowship. The authors are grateful to acknowledge the contributions and advice of Hector Medecki and David Attwood.

References

1. W. P. Linnik, "A Simple Interferometer for the Investigation of Optical Systems," Proceedings of the Academy of Sciences of the USSR 1, 208 (1933).
2. R. N. Smartt, W. H. Steel, "Theory and application of point-diffraction interferometers (telescope testing)," Japan. J. of Appl. Phys. 14 (Suppl. 14-1), 351 (1975).
3. R. J. Speer, M. Chrisp, D. Turner, *et al*., "Grazing incidence interferometry: the use of the Linnik interferometer for testing image-forming reflection systems," Appl. Opt. 18 (no. 12), 2003-12 (1979).
4. H. Medecki, E. Tejnil, K. A. Goldberg, J. Bokor, "A Phase-Shifting Point Diffraction Interferometer," *accepted for publication in Optics Letters.*
5. K. A. Goldberg, R. Beguiristain, J. Bokor, *et al.,* "Progress towards λ/20 extreme ultraviolet interferometry," J. Vac. Sci. & Tech. B 13 (no. 6), 2923-27 (1995).
6. E. Tejnil, K. A. Goldberg, J. Bokor, *et al.*, "Phase-shifting point diffraction interferometry for at-wavelength testing of lithographic optics," these proceedings.
7. C. Cerjan, "Scalar wave diffraction from a circular aperture," in OSA Proceedings on Extreme Ultraviolet Lithography, F. Zernike, D. T. Attwood, eds. (Optical Society of America, 1994), Vol. 23.
8. M. Born, and E. Wolf, Principles of Optics, 6th ed., Chp. 8, (Pergamon Press, NY, 1980).
9. J. P. Spallas, R. E. Hostetler, G. E. Sommargren, D. R. Kania, "Fabrication of extreme-ultraviolet point-diffraction interferometer aperture arrays," Appl. Opt. 34 (no. 28), 6393-8 (1995).
10. A. K. Wong, A. R. Neureuther, "Rigorous three-dimensional time-domain finite-difference electromagnetic simulation for photolithographic applications," IEEE Transactions on Semiconductor Manufacturing 8, 419-31 (1995).
11. R. H. Clarke and J. Brown, Diffraction Theory and Antennas, p. 85, (John Wiley & Sons, NY 1980).
12. Code V Reference Manual, v 8.0, p. 2A-335, Optical Research Associates, Pasadena, CA.
13. D. J. Fischer, J. T. O'Bryan, *et al.,* "Vector formulation for interferogram surface fitting," Appl. Opt. 32 (no. 25), 4738-43 (1993).